



Open Archive Toulouse Archive Ouverte (OATAO)

OATAO is an open access repository that collects the work of Toulouse researchers and makes it freely available over the web where possible.

This is an author-deposited version published in: <http://oatao.univ-toulouse.fr/>
Eprints ID : 2407

To link to this article :

URL : <http://dx.doi.org/10.1149/1.2969277>

To cite this version : Boisier, Grégory and Pébère, Nadine and Druetz, Catherine and Villatte, Martine and Suel, Stéphane (2008) [*FESEM and EIS Study of Sealed AA2024 T3 Anodized in Sulfuric Acid Electrolytes: Influence of Tartaric Acid.*](#) Journal of The Electrochemical Society (JES), vol. 155 (n° 11). C521-C529. ISSN 0013-4651

Any correspondence concerning this service should be sent to the repository administrator: staff-oatao@inp-toulouse.fr

FESEM and EIS Study of Sealed AA2024 T3 Anodized in Sulfuric Acid Electrolytes: Influence of Tartaric Acid

Grégory Boisier,^{a,*} Nadine Pébère,^{a,**,z} Catherine Druetz,^b Martine Villatte,^b and Stéphane Suel^b

^aInstitut Carnot CIRIMAT/UMR CNRS 5085, ENSIACET, 31077 Toulouse Cedex 04, France

^bEADS IW, 92152 Suresnes Cedex, France

The present study investigates the effect of tartaric acid on anodic film morphology and on corrosion resistance of hydrothermally sealed anodized AA2024. Anodizing treatment was performed in dilute sulfuric acid electrolyte with or without addition of tartaric acid. Hydrothermal sealing was carried out in boiling water for each anodized specimen. The morphology of the sealed anodic films was examined using field-emission scanning electron microscopy (FESEM). Electrochemical impedance spectroscopy (EIS) was performed to assess sealing quality and corrosion resistance of the anodic films. It was shown that the sealing was more efficient in the case of anodic films formed in tartaric acid electrolyte mainly due to their lower porosity. It was also observed that the properties of the barrier layer were higher when sealing was performed on specimens anodized in the presence of tartaric acid. This suggests a specific role of the species on the barrier layer, which contributes to the enhancement of the performance in terms of corrosion resistance of the sealed anodic films. The present study clearly validates the beneficial role of tartaric acid in anodizing baths for the corrosion protection of AA2024.

[DOI: 10.1149/1.2969277]

Chromic acid (CA) anodizing is widely used in the aeronautic industry to improve corrosion resistance of aluminum alloys.¹ The incorporation of Cr(VI) and Cr(III) into the oxide gives higher corrosion resistance than that produced by other anodizing processes. Since the beginning of the 1990s, the high toxicity associated with Cr(VI) has imposed restrictions on their use in industrial applications. As a consequence, numerous attempts have been made to find less toxic alternatives, but with limited success.^{2,3} During the last decade, attention to sulfuric acid anodizing and boric-sulfuric acid anodizing as alternatives to replace CA anodizing has increased.⁴⁻⁶ Anodizing with more dilute sulfuric acid (DSA) has been introduced to obtain thin anodic films (1–5 μm) that increase fatigue resistance for specific structural materials.⁷ Even though the fatigue resistance of the specimens anodized in DSA are increased, the corrosion resistance is lower than that of specimens anodized in CA. Alenia Aeronautica S.P.A. has proposed a new anodizing procedure involving the addition of tartaric acid in dilute sulfuric acid electrolyte, called tartaric-sulfuric acid (TSA) anodizing.⁸ Tartaric acid is sometimes used as anodizing electrolyte for pure aluminum due to its ability to form anodic films with self-ordered pores.^{9,10} However, the use of TSA mixtures as anodizing electrolytes is poorly reported in the literature. Iglesias-Rubianes et al. have investigated the influence of the addition of tartaric acid to sulfuric acid electrolyte on anodizing of sputtering-deposited Al–Cu alloy and AA2024-T3 alloy.¹¹ The authors showed that the addition of tartaric acid reduced by ~20% the steady-state current during film growth at constant voltage. Transmission electron microscopy (TEM) observations showed that the presence of tartaric acid in the anodizing bath did not change the film morphology. Marzocchi et al. observed similar trends when investigating the anodizing of AA2024-T3 in a DSA (0.46 M) solution and in an alternative sulfuric (0.46 M) + tartaric acid (0.53 M) solution.¹² The authors concluded that the morphology of the anodic films formed in the two solutions was similar. Neither of the research groups attempted to investigate corrosion behavior.^{11,12} The role of tartaric acid in the anodizing bath still remains unclear.

The present study aimed for a better understanding of the effect of tartaric acid on the anodic film morphology and on the corrosion resistance of hydrothermally sealed anodized AA2024. Anodizing treatment was performed in DSA electrolyte with (TSA) or without (DSA) addition of tartaric acid. Hydrothermal sealing was carried

out in boiling deionized (DI) water for each anodized specimen. The morphology of the unsealed and hydrothermally sealed anodic films was examined using field-emission scanning electron microscopy (FESEM). FESEM was found to be a powerful tool to visualize changes in oxide film morphology after anodizing and sealing treatments.^{5,9,13-15} Electrochemical impedance spectroscopy (EIS) was carried out to characterize the properties of the sealed and unsealed anodic films. The sensitivity of EIS makes it a successful technique for assessing the sealing quality and corrosion resistance of the anodic films.^{5,12,14,16-21} The electrochemical parameters obtained from a fitting procedure of the impedance diagrams allowed the corrosion behavior difference of the two specimens to be shown and discussed. The electrochemical results were correlated with the FESEM observations.

Experimental

Materials and conditions.—The material used was a 2024 T3 aluminum alloy. The average chemical composition of the alloy is given in Table I. The specimens consisted of 125 \times 80 \times 1.6 mm plates machined from an AA2024 T3 rolled plate. Before anodizing, the samples were degreased (pH 9) for 15 min and then etched in an acid bath at 35 °C for 10 min. Anodizing treatment was performed in a 40 g L⁻¹ (0.41 M) sulfuric acid (H₂SO₄) solution in the presence or absence of 80 g L⁻¹ (0.53 M) tartaric acid (C₄H₆O₆). Anodizing experiments were carried out at a constant cell voltage of 14 V for 20 min reached after a 5 min voltage ramp. The operating temperature was fixed at 37 °C. Sealing was carried out in DI water (ρ > 1500 k Ω cm) at a temperature of >96 °C.

Scanning electron microscope (SEM) observations.—The morphology of the anodic layers was investigated before and after sealing using an LEO 435 VP SEM. For higher-resolution observations, a JEOL JSM 6700F FESEM was used. Sealed and unsealed anodized specimens were coated with a 1 nm thick layer of platinum to reduce the charging effect on the surface observed and thus to improve the image quality.

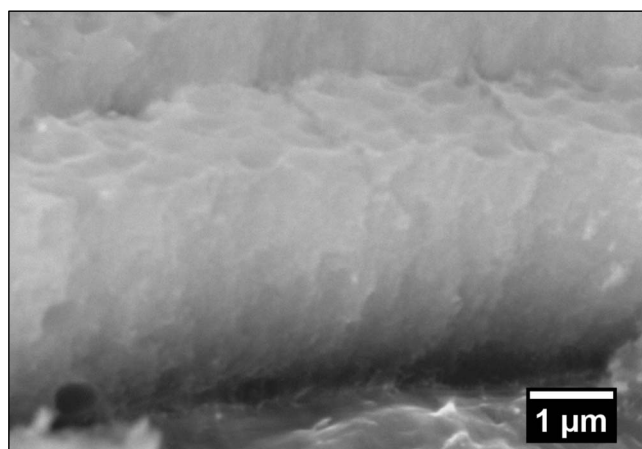
Table I. Chemical composition (in weight percent) of 2024 T3 aluminum alloy.

Cu	Mg	Mn	Si	Fe	Zn	Ti	Al
4.50	1.44	0.60	0.06	0.13	0.02	0.03	Bal.

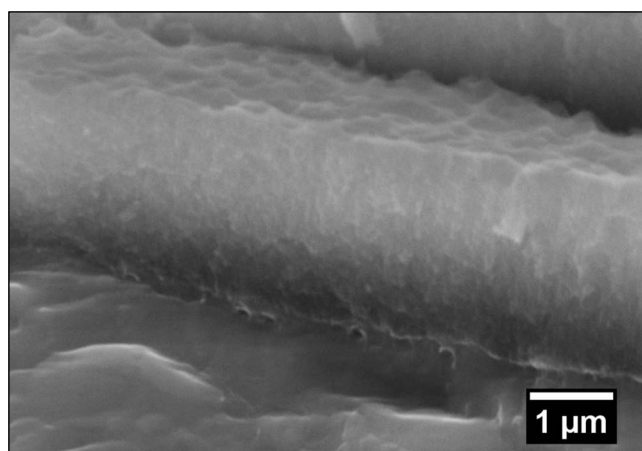
* Electrochemical Society Student Member.

** Electrochemical Society Active Member.

^z E-mail: Nadine.Peber@ensiacet.fr



(a)



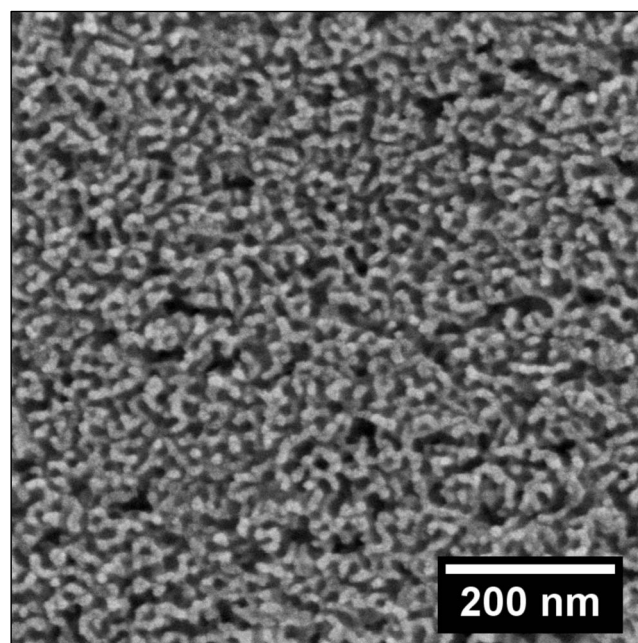
(b)

Figure 1. SEM observations of cross sections of unsealed anodic films formed in (a) DSA and (b) TSA solutions.

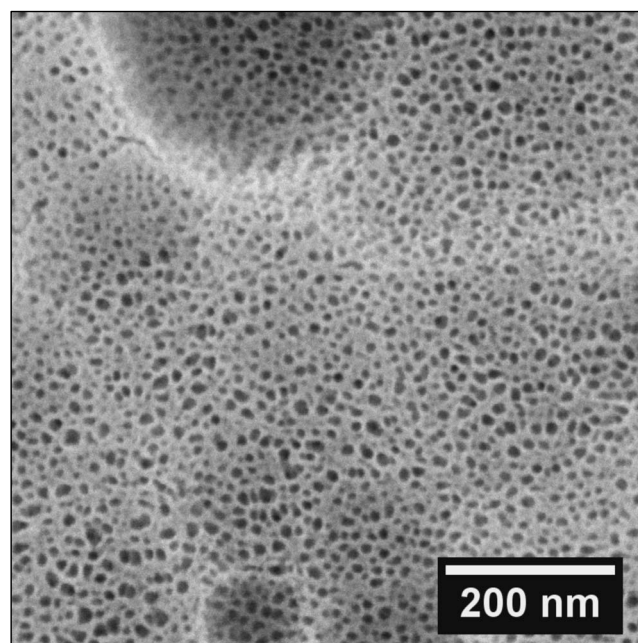
Electrochemical experiments.— A three-electrode electrochemical cell was used. It contained a platinum grid as auxiliary electrode (area of $\sim 30 \text{ cm}^2$), a saturated calomel reference electrode, and the anodized AA2024 T3 specimens as working electrode (exposed area of 28 cm^2). Electrochemical impedance measurements were carried out using a Solartron 1287 electrochemical interface and a Solartron 1250 frequency response analyzer. The impedance diagrams were plotted under potentiostatic conditions at the corrosion potential over a frequency range of 65 kHz to 9.54 mHz with 6 points per decade. The electrochemical cell was kept at room temperature and open to air. The electrochemical properties of the unsealed anodic films were characterized after 2 h of immersion in a 0.5 M Na_2SO_4 solution. Sodium sulfate was chosen for its low corrosiveness toward aluminum and aluminum alloys. The corrosion behavior of sealed anodic films was investigated in a 0.5 M NaCl solution, at different exposure times reaching 35 days (840 h).

Results and Discussion

Characterization of the anodic films.— Figure 1 shows the SEM micrographs of cross sections of unsealed AA2024 T3 specimens anodized in DSA (Fig. 1a) and in TSA electrolytes (Fig. 1b). The anodic layer thickness was 2.9 and $2.4 \mu\text{m}$ for the anodic films formed in DSA and TSA, respectively. Figure 2 shows the FESEM images of the surface of unsealed anodic film formed in DSA (Fig. 2a) and TSA (Fig. 2b). The porous oxide layer morphology appears differently. For the anodic film formed in DSA, the pores are not well defined and the distribution is irregular. Some pores seem to



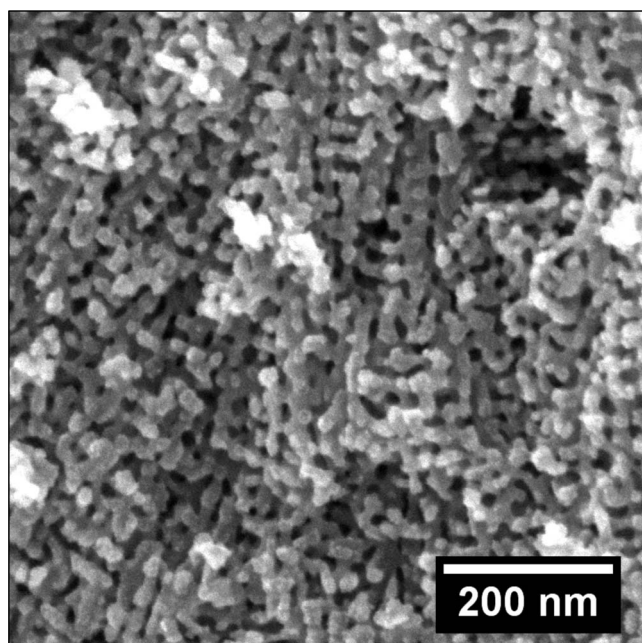
(a)



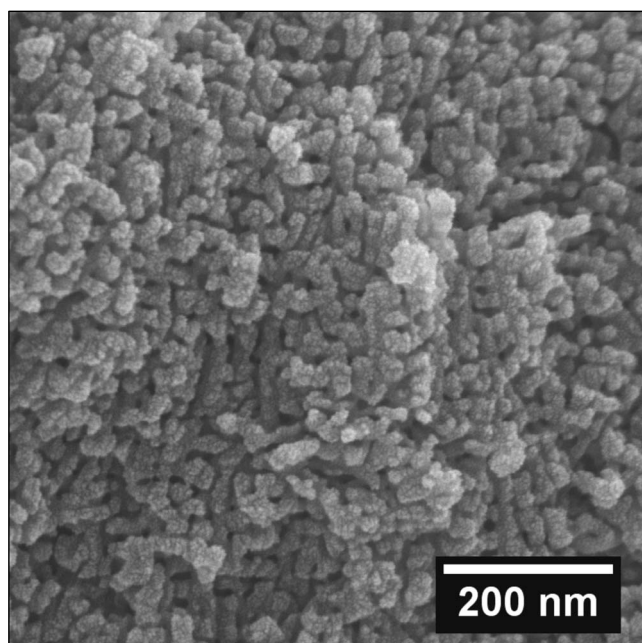
(b)

Figure 2. FESEM observations of the surface of unsealed anodic films formed in (a) DSA and (b) TSA solutions.

have coalesced, because in some parts of the surface, the distance between the pore walls reaches about 30–40 nm. For the anodic films formed in TSA (Fig. 2b), the pores are well distributed and appear to be better organized. The average pore diameter varied between 10 and 15 nm. From the surface observations, the pore volume seems to be higher in the case of the anodic film formed in DSA. FESEM observations of film cross sections (Fig. 3) corroborate these assumptions. The area between pore walls (in black) is larger for the anodic film formed in DSA than for the film formed in TSA. High tortuosity of the internal porous structure is observed for both types of anodic films, which is the characteristic morphology of films formed on 2XXX series aluminum alloys. The coarse intermetallic particles and the presence of alloying elements in the alumi-



(a)



(b)

Figure 3. FESEM observations of cross sections of unsealed anodic films formed in (a) DSA and (b) TSA solutions (zone in the bulk of the oxide layer).

num matrix significantly modify the anodic film morphology.²² Particularly, the Cu present in solid solution oxidizes and leads to the generation of oxygen bubbles during film growth, inducing film disruptions. The changing directions of pores propagation contribute to the three-dimensional (3D) aspect of the pore morphology.²³⁻²⁸ The morphology encountered from the metal-oxide interface all the way up to the upper part of the oxides was the same (not shown).

FESEM observations revealed that the presence of tartaric acid decreased the pore volume of the anodic film. Tartaric acid is known to be a weak acid, not very aggressive toward the metal and its oxide, which requires high temperature and voltage (>150 V) to produce a dissolving action similar to that of sulfuric acid.^{9,10,29-31}

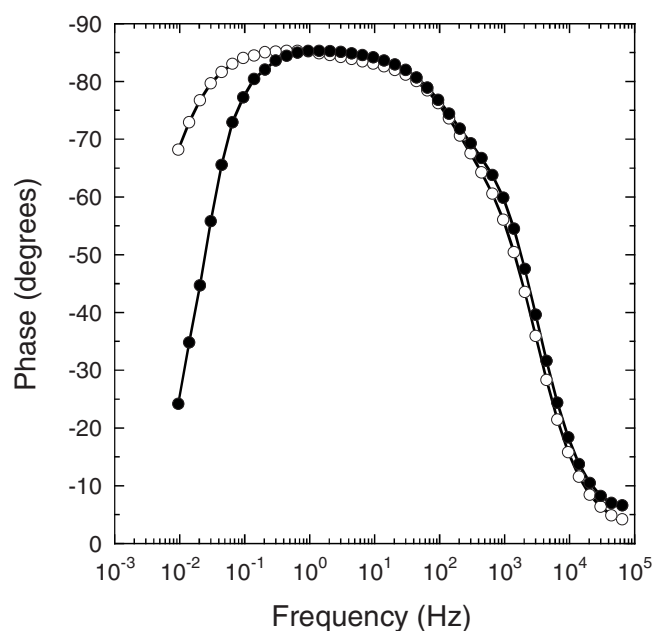
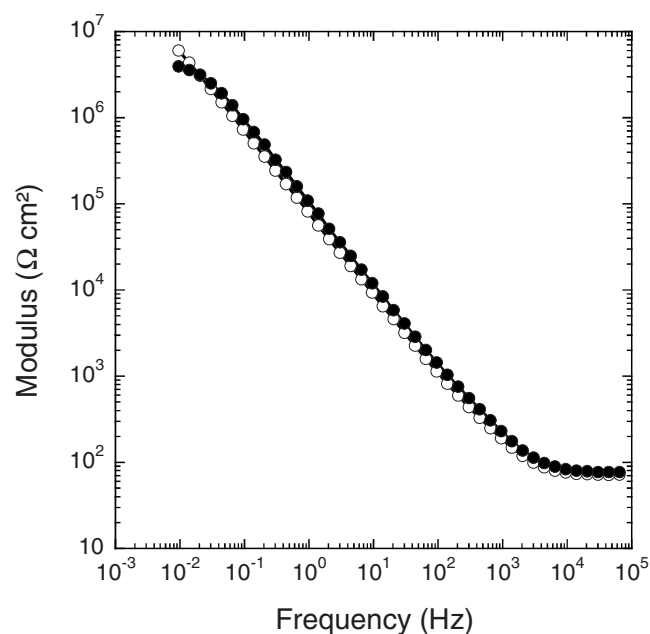


Figure 4. Bode plots of the unsealed anodic films formed in (○) DSA and in (●) TSA solutions (obtained after 2 h of immersion in 0.5 M Na₂SO₄).

As a consequence, it is obvious that tartaric acid cannot contribute to the formation of the anodic film at the voltage applied (14 V) and that sulfuric acid is the main reservoir of mobile protons involved in the growth of the oxide layer. Because all the anodizing parameters were the same for both systems, the decrease in pore volume observed for the anodic film formed in TSA may be attributed to a decrease of the dissolution rate occurring at the pore base during pore formation. It can be assumed that tartaric acid influences the field-assisted dissolution process during pore initiation as proposed by Iglesias-Rubianes et al., limiting the dissolution of the outwardly mobile Al³⁺ species present in the pore precursor sites.¹¹

The electrochemical behavior of both unsealed anodic layers was investigated by impedance spectroscopy. The diagrams obtained after 2 h of immersion in a 0.5 M Na₂SO₄ solution for the anodic films formed in DSA and TSA are presented in Fig. 4. The spectra are relatively similar, except in the low-frequency range, and present

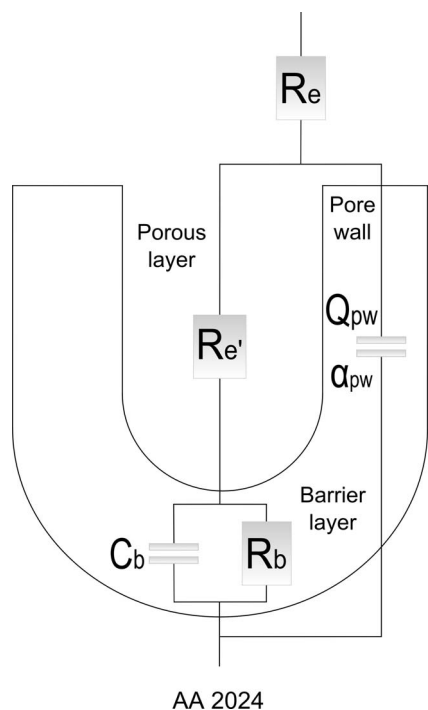


Figure 5. Equivalent circuit used to model the electrochemical behavior of unsealed anodic films (R_e : electrolyte resistance, R_e' : resistance of the solution in the pores, R_b : barrier layer resistance, C_b : capacitance associated to the barrier layer, and Q_{pw} and α_{pw} : CPE parameters associated to the pore wall).

two time constants that are not well separated. The time constant in the high-frequency part of the diagram (characteristic frequency at $\sim 10^3$ Hz) is assumed to represent the response of the pore walls, and the low-frequency part is attributed to the barrier layer.^{16-18,20} An equivalent circuit containing two time constants (Fig. 5) was needed to fit the data as proposed by Hoar and Wood.¹⁶ For the pore wall, constant phase element (CPE) was introduced instead of capacitance (with α close to 0.90).³² For the barrier layer, α parameters were close to 1 (0.94–0.99), and thus, a capacitance, C_b , was used in the circuit. For the sake of simplicity, only the parameters associated to the barrier layer are reported in Table II. The results show a higher R_b value for the anodic film formed in DSA than for the anodic film formed in TSA. This shows that the barrier layer is affected by the presence of tartaric acid in the anodizing bath. For both unsealed anodic films, the barrier layer thickness e_b can be calculated with the following expression that defines capacitance

$$C_b = \frac{\epsilon_0 \epsilon_r S}{e_b} \quad [1]$$

with the dielectric permittivity of vacuum $\epsilon_0 = 8.854 \times 10^{-14}$ F cm⁻¹, the relative dielectric constant of alumina $\epsilon_r = 10$, and the exposed surface area S . Calculations of e_b from Eq. 1 gave: 21 and 25 nm for the anodic films formed in DSA and TSA, respec-

Table II. Fitted parameter values associated to the barrier layer and corresponding thickness, for the unsealed anodic films formed in DSA and in TSA solutions (obtained after 2 h of immersion in 0.5 M Na₂SO₄).

	R_b (M Ω cm ²)	C_b (μ F cm ⁻²)	e_b (nm)
DSA	22	0.41	21
TSA	6	0.35	25

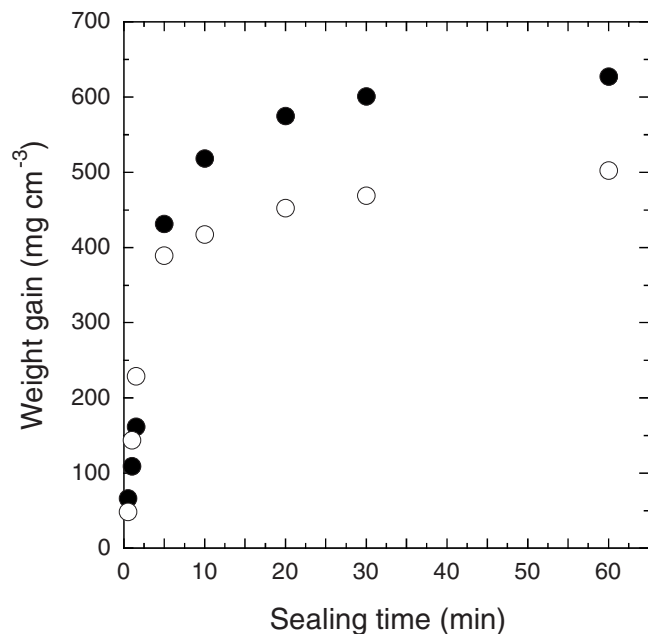


Figure 6. Variation of weight gain with sealing time in boiling DI water for anodic films formed in (○) DSA and (●) TSA solutions.

tively, which is in good agreement with the values reported by Marzocchi et al. [17 nm (DSA) and 23 nm (TSA) measured by TEM].¹² The higher R_b value of the anodic film formed in DSA cannot be explained by a greater thickness of the barrier layer. This disagreement may be due to the dielectric properties of the barrier layer, which are affected by the presence (or not) of tartaric acid in the anodizing electrolyte. Further investigations to determine the action of tartaric acid on the barrier layer would be necessary. The results show that the porous structure of the anodic films differs with the anodizing electrolyte; thus, the sealing of the pores in boiling water may give different results in terms of pore-filling quality and, therefore, in terms of corrosion resistance.

Characterization of the hydrothermal sealing mechanism.—

Figure 6 presents the variation of the weight gain with the sealing time in boiling DI water for the anodic films formed in DSA and TSA. The weight gain is expressed vs anodic film volume by taking into account the initial thickness of the anodic films. In agreement with the literature, the curves present the usual parabolic shape and can be divided into two domains.³³⁻³⁷ During the initial step (0–90 s), a high rate of sealing of ~ 150 mg cm⁻³ min⁻¹ for the anodic film formed in DSA and a lower rate of sealing of ~ 100 mg cm⁻³ min⁻¹ for the anodic film formed in TSA was observed. Then, it slowed down to ~ 1 mg cm⁻³ min⁻¹ between 20 and 60 min of sealing for both anodic films. These results highlight the significant transformation of the porous structure occurring in the early stages of the sealing process for both types of anodic film. The significant difference in sealing rates observed at the beginning of the reaction corroborates the higher porosity of the anodic film formed in DSA previously observed by FESEM. Indeed, the higher the available surface area (pore volume) is, the faster the initial water uptake and the greater the weight gain is. Furthermore, after a longer sealing time (>20 min), a difference in weight gain was observed between the anodic films. For 60 min of sealing, the weight gain reached 630 and 500 mg cm⁻³ for the anodic films formed in TSA and DSA, respectively. This shows that the precipitation of aluminum hydroxide was greater in the anodic film formed in TSA, suggesting a more complete sealing of the porous structure than for the anodic films formed in DSA.

FESEM observations of the surface of anodic films formed in TSA after different sealing times corroborated the variation of

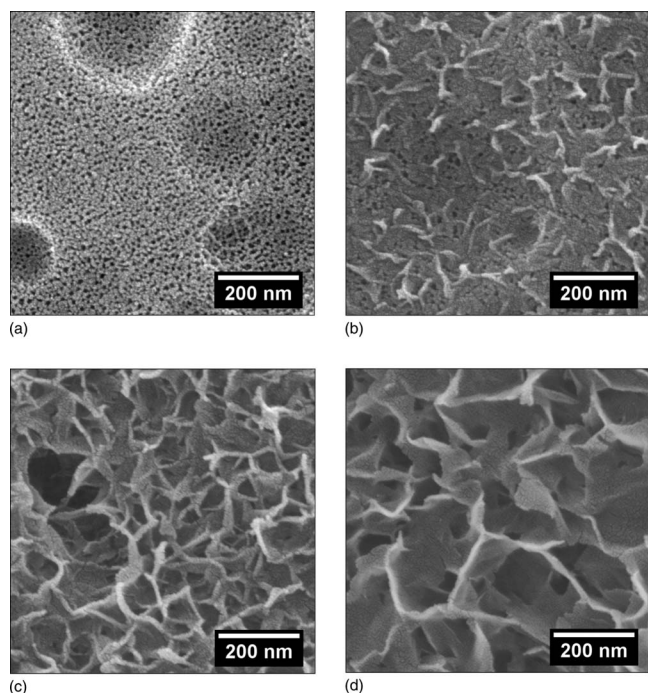


Figure 7. FESEM observations of the surface of anodic films formed in TSA solution after different sealing times in boiling water: (a) 30 s, (b) 60 s, (c) 90 s, and (d) 5 min.

weight gain (Fig. 7). After 30 s of reaction (Fig. 7a), a reduction of pore diameter is clearly seen since the upper part of the pore walls has swollen. After 60 s of sealing (Fig. 7b), the formation of a very short “plug” in the pore mouths and the growth of “petal”-shaped crystals are clearly observed. Then, 90 s of sealing (Fig. 7c) induce the quasi-plugging of the pore mouths. For the longest sealing times (Fig. 7d), a dense layer of these crystals is present on the surface and only grows slightly after 5 min of reaction. Similar modifications were observed after short and long sealing times of the anodic films formed in DSA (not shown). After long sealing times, both anodic film surfaces presented a dense layer of acicular crystals. The observation of pore sealing is in good agreement with the literature. Initial dissolution of the pore walls is followed by diffusion and precipitation of aluminum hydroxide on the pore mouths leading to the formation of a plug in the upper part of the pore, which greatly restricts the transfer of water molecules down the entire length of the pores.^{13,16,33-39} The formation of petal-shaped crystals on the surface, so-called smudge, is the result of aluminum salt precipitation.^{2,14,15,36,37,39} According to Wefers, the chemical nature of the crystals seems to be close to pseudoboehmite or boehmite and their morphology reflects the chemical and thermal conditions prevailing during the sealing treatment.^{36,37}

The various transformations of the porous structure occurring during the sealing process were evaluated by impedance spectroscopy for both types of anodic film. First, the results obtained with the anodic films formed in TSA are presented and then the results obtained for films formed in DSA. Figure 8 shows the impedance diagrams obtained after 2 h of immersion in a 0.5 M NaCl solution for the anodic films formed in TSA and for different sealing times in boiling DI water. They are characterized by two time constants. Several studies have shown that the physical transformations involved during sealing are reflected in the high- and medium-frequency ranges of the impedance diagrams by the appearance of a new time constant, which characterizes the sealed porous layer properties, while the barrier layer properties are characterized in the low-frequency range.^{5,12,14,16-21} The impedance data were analyzed by different equivalent circuits.^{16,17,20} The circuit that gave the best

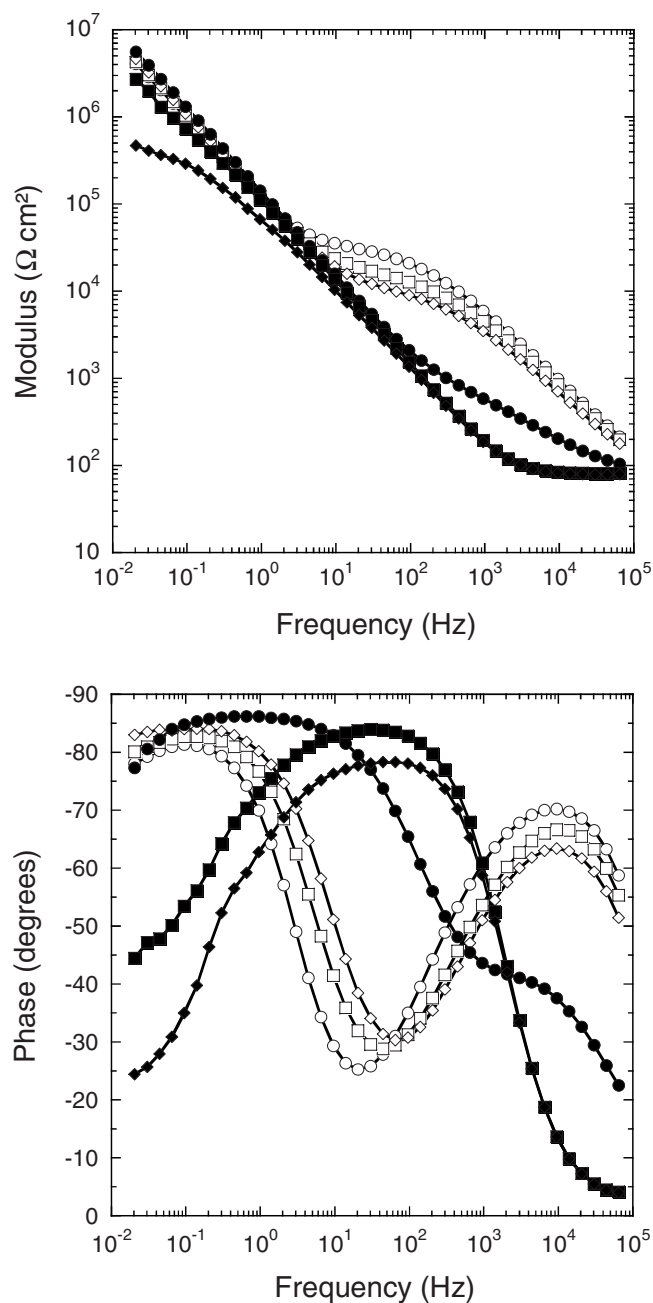


Figure 8. Bode plots of anodic films formed in TSA solution sealed after different times in boiling DI water: (◆) 30 s, (■) 90 s, (●) 2 min, (◇) 5 min, (□) 20 min, and (○) 60 min (obtained after 2 h of immersion in 0.5 M NaCl).

fits is presented in Fig. 9. It is relatively similar to the one proposed by González et al. with the difference that the intermediate layer and pore wall resistances were respectively too low and too high, and have been deleted because they do not contribute to improve the fitting quality of our experimental data.²⁰ It can be noted that for 30 and 90 s of sealing, the impedance diagrams are typical of unsealed (partially sealed) materials, and thus, the electrochemical parameters are extracted only from 2 min of sealing (Table III). The resistance R_p , which gives an indication of the sealing quality, increases with the sealing time. The longer the sealing time is, the better the sealing quality is. At least 5 min of sealing are required to obtain sufficient filling of the pores, which corresponds to the transition between the high and low rates of weight gain observed in Fig. 6. However, R_p increased progressively with the sealing time while the weight gain

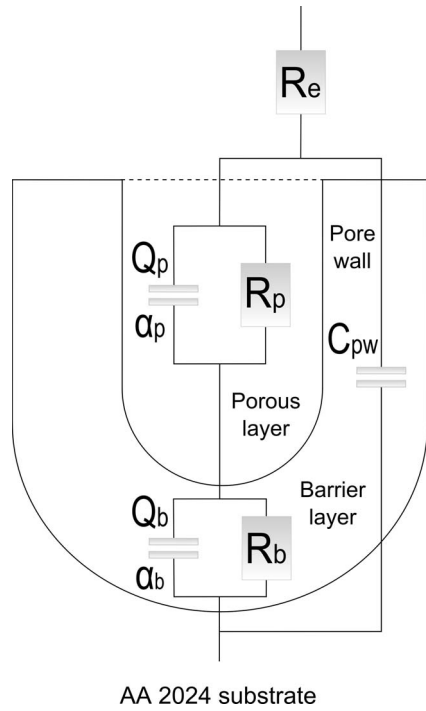


Figure 9. Equivalent circuit used to model the electrochemical behavior of sealed anodic films (R_e : electrolyte resistance, R_p : porous layer resistance, Q_p and α_p : CPE parameters associated to the porous layer, R_b : barrier layer resistance, Q_b and α_b : CPE parameters associated to the barrier layer, and C_{pw} : capacitance associated to the pore wall).

slowed down and stabilized. Thus, the decrease of the residual porosity by successive precipitation of aluminum hydroxide has a significant influence on the resistivity of the porous layer. α_p values are low, independently of the sealing time. To analyze this parameter more accurately, it would be necessary to consider a transmission line model to take into account the porous structure.⁴⁰ From Table III, it can be seen that R_b , Q_b , and α_b remain quasi-constant, whatever the sealing time.

The impedance diagrams obtained after different sealing times (5, 10, 20, and 30 min) for the anodic films formed in DSA (not shown) have the same shape as those obtained for the films formed in TSA. Figure 10 compares the R_p values for both systems. It appears that for the anodic films formed in TSA, the variation is linear; whereas for the films formed in DSA it is not, and the R_p values always remain lower than those obtained with TSA. For the shortest sealing time, R_p was $<5 \text{ k}\Omega \text{ cm}^2$, which reveal the low level of pore filling. Sealing times of $>30 \text{ min}$ are necessary to obtain acceptable sealing of the porous structure. FESEM observations of cross sections of sealed films formed in DSA and TSA (Fig. 11) were performed to observe possible morphology differences of the sealed porous layer, which could explain the differences in R_p values. The micrographs reveal differences only in the zone adjacent

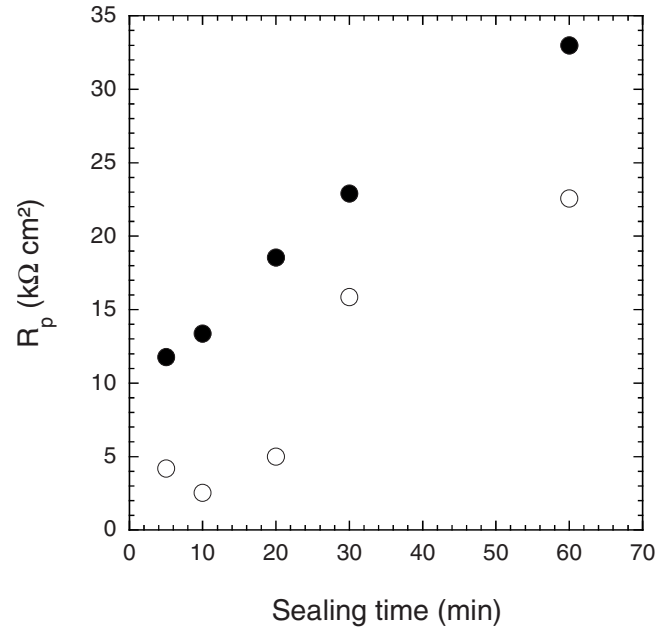


Figure 10. R_p values vs sealing time for the anodic films formed in (○) DSA and (●) TSA solutions.

to the base metal. The sealed layer of the anodic films formed in TSA (Fig. 11b) appears as a dense block, where the initial porosity and pore structure are no longer distinguishable. The sealed layer of the anodic films formed in DSA (Fig. 11a) appear to be less dense, in parts. Fine acicular particles coming from aluminum hydroxide precipitation are clearly observable, surrounded by a small proportion of dark areas, which can be assimilated to residual porosity. These observations show that the lower part of the porous structure of the anodic film formed in DSA was not perfectly sealed after 30 min of reaction, corroborating the trends deduced from electrochemical impedance results.

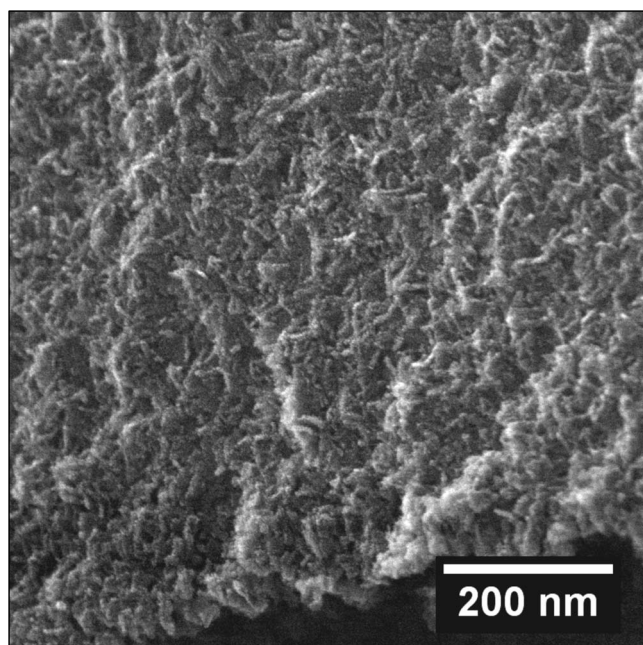
The impedance results stress that pore sealing differs, depending on the initial anodic film. A better sealing efficiency (higher R_p) was obtained for the anodic films formed in the presence of tartaric acid. Then, to investigate the influence of sealing quality on the corrosion of sealed anodized AA2024 specimens, the corrosion resistance of the sealed anodic films formed in DSA and TSA was investigated by plotting the impedance diagrams vs exposure time (from 2 to 840 h) in a 0.5 M NaCl solution.

Characterization of corrosion resistance of sealed specimens.—

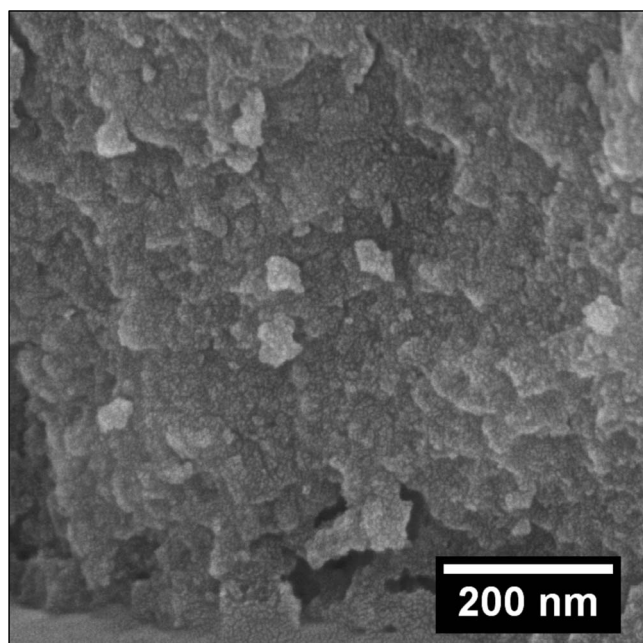
Figure 12 shows a 3D plot of the fitted R_p values for the anodic films formed in TSA and for different sealing times as a function of exposure time in a 0.5 M NaCl solution. The results obtained for the specimens anodized in DSA and sealed in boiling DI water for 20, 30, and 60 min are reported for comparison. For the anodic films formed in TSA, R_p decreases as the exposure time in the aggressive solution increases for each sealing time, except for the specimen

Table III. Fitted parameter values for the hydrothermally sealed anodic films formed in TSA solution (obtained after 2 h of immersion in 0.5 M NaCl).

Sealing time (min)	R_e ($\Omega \text{ cm}^2$)	R_p ($\text{k}\Omega \text{ cm}^2$)	Q_p ($\mu\Omega^{-1} \text{ cm}^{-2} \text{ s}^\alpha$)	α_p	R_b ($\text{M}\Omega \text{ cm}^2$)	Q_b ($\mu\Omega^{-1} \text{ cm}^{-2} \text{ s}^\alpha$)	α_b	C_{pw} (nF cm^{-2})
2	78	1.1	16.74	0.52	~34	1.21	0.96	28.5
5	81	11.8	0.83	0.63	~133	1.49	0.95	11.7
10	85	13.4	0.92	0.60	~15	1.56	0.94	12.4
20	84	18.6	0.76	0.60	~56	1.56	0.94	11.5
30	81	22.9	0.56	0.62	~48	1.55	0.94	10.6
60	79	33.0	0.32	0.67	~38	1.62	0.94	9.3



(a)



(b)

Figure 11. FESEM observations of cross sections of anodic films formed in (a) DSA and (b) TSA solutions, after 30 min of sealing in boiling DI water (zone adjacent to the base metal).

sealed for 60 min. The decrease of R_p values during the first 336 h of immersion indicates penetration of the electrolyte and an enhancement of the ionic conduction along the pores by degradation of the sealed porous layer.^{18,19} The R_p value of the specimen sealed for 60 min remains high and constant during the first 336 h of immersion, which indicates that 60 min of sealing induces a strong densification of the porous layer preventing electrolyte penetration during a longer time than for the other specimens. With specimens sealed for 5, 10, 20, and 30 min, a slight increase of R_p can be seen after 840 h of immersion. This is attributed to a self-sealing mechanism occurring after a long contact time with the water molecules at room temperature. For the anodic films formed in DSA, the variation of

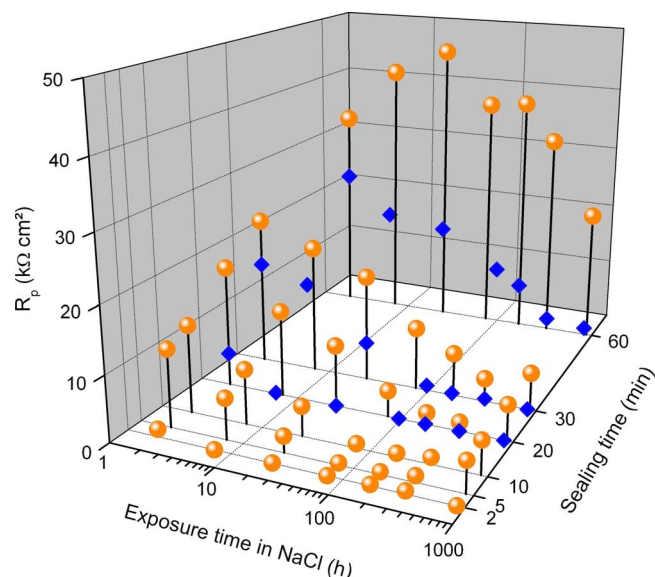


Figure 12. (Color online) R_p values for the anodic films formed in (◆) DSA and (gray circle) TSA solutions vs sealing times and vs exposure time in a 0.5 M NaCl solution.

R_p is similar but with a sharper decrease. After only 6, 96, and 336 h of immersion in the aggressive solution for the specimens sealed for 20, 30, and 60 min, respectively, the time constant associated to the sealed porous layer completely vanishes. Moreover, no self-sealing phenomenon is observed for longer immersion times. The fast decrease of R_p stresses the fact that the sealed layers of the anodic films formed in DSA are less compact than those of anodic films formed in TSA.

Figure 13 presents the variation of the fitted R_b values as a function of exposure time in the 0.5 M NaCl solution for 20 and 30 min sealed anodic films formed in TSA and DSA. The R_b values obtained for the anodic films formed in TSA are high and remain constant for the first 336 h of immersion, indicating that the barrier layer is unattacked. This is consistent with the fact that the porous layer is homogeneously sealed along the entire length of the pores, preventing the degradation of the barrier layer. In contrast, the R_b values obtained for the anodic films formed in DSA remain relatively constant only during the first 96 h of immersion and then decrease sharply, indicating a significant degradation of the barrier layer due to the low protection afforded by the sealed porous layer. Furthermore, Fig. 13 shows that after a short immersion time in the aggressive solution, the R_b values obtained for the sealed films formed in DSA were lower by about one order of magnitude compared to sealed films formed in TSA. These differences can be attributed to a modification of the barrier layer by sealing when the alloy is anodized in the presence of tartaric acid. Thus, the corrosion protection afforded by sealing on anodic films formed in DSA does not last as long as that gained with anodic films formed in TSA.

Discussion.— The present study highlights that the corrosion resistance of sealed specimens was significantly enhanced when the alloy was anodized in the electrolyte containing tartaric acid. Comparison of the EIS measurements showed differences between the anodic films concerning both the sealing quality and the barrier layer properties. A drastic fall of R_p and a progressive decrease of R_b during immersion in the NaCl solution was observed for the sealed anodic films formed in DSA, accounting for surface degradation, whereas the anodic films formed in TSA showed higher R_p and R_b values during the whole immersion time, indicating a higher corrosion resistance. These results are the consequence of the more efficient sealing of the porous structure of the anodic films formed with tartaric acid.

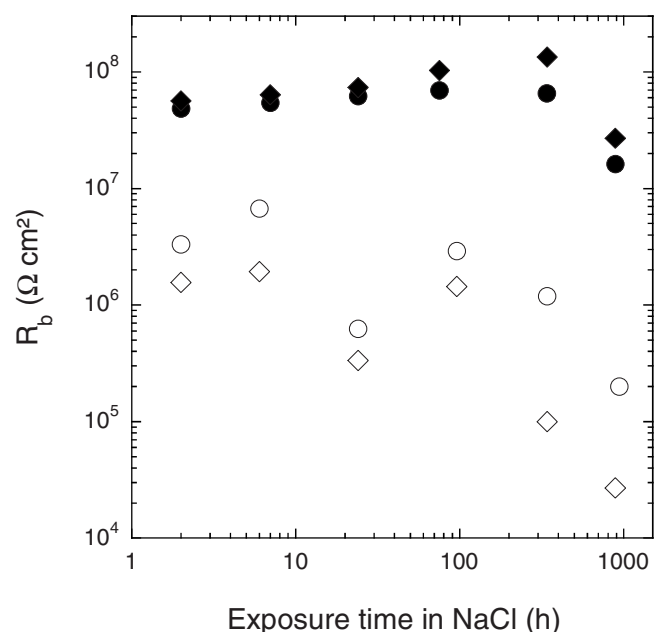


Figure 13. R_b values for the anodic films formed in DSA after two different sealing times (◇) 20 min and (○) 30 min and for the anodic films formed in TSA after two different sealing times (◆) 20 min and (●) 30 min vs exposure time in a 0.5 M NaCl solution.

FESEM image (Fig. 2 and 3) clearly show a lower porosity of the anodic films formed in TSA by comparison to the anodic films formed in DSA. Moreover, the variation of weight gain during sealing in boiling DI water revealed that the initial rate is lower for the anodic films formed in TSA, which is in agreement with their lower porosity. It is well known that the sealing reaction begins in the external part of the pore by the formation of a plug, decreasing water molecule transfer.^{13,16,33-39} Radial displacement of the pore walls toward the pore center continues due to crystallization of aluminum hydroxide. It is obvious that the lower the initial pore diameter is, the faster the pores will be filled to reach complete closing. Consequently, the lower pore diameter observed for the anodic film formed in TSA contributes to better pore filling compared to the film formed in DSA.

In addition, a difference in chemical composition of the anodic films should be taken into account. Although the two anodic films formed in DSA and TSA may have a similar proportion of sulfate ions incorporated in their porous structure, the main difference arises from the use of tartaric acid in the anodizing bath, which may also induce incorporation of tartarate anions into the porous structure.^{33-37,41} Some of the incorporated species are released via dissolution of the pore walls during the initial step of the sealing process.^{13,33-37,39} The presence of such species in the electrolyte can influence the rate of the sealing reaction.³³⁻³⁷ In the present study, the hydrolysis of aluminum salt (formed with tartarate anions) by reaction with water may account for the more efficient sealing obtained with the anodic film formed in TSA. It can be assumed that chemical conditions inside the pores, such as pH, are more favorable for aluminum hydroxide precipitation when tartarate salts are hydrolyzed in addition to sulfate salts. Thus, the combination of the chemical action of tartaric acid during sealing and the lower porosity of the anodic film may contribute to the better sealing of the pores of the anodic film formed in TSA.

From Fig. 13, differences in terms of barrier layer resistance can be seen. Tartaric acid may be involved in barrier layer modification occurring on sealing of the anodic films formed in TSA, but its specific action remains unclear and requires further investigations. However, the enhancement of barrier layer resistance must be taken into account to explain the better corrosion resistance observed for

the sealed films formed in TSA because a porous layer correctly sealed is not sufficient to ensure high performance in terms of corrosion resistance.

Conclusion

The sealing quality and the corrosion resistance of AA2024 T3 anodized in sulfuric acid with or without addition of tartaric acid were investigated by FESEM and EIS techniques. The following points emerged:

1. Anodizing of AA2024 T3 in the presence of tartaric acid led to the formation of anodic films with lower porosity than those obtained in DSA.
2. Characterization of hydrothermal sealing by EIS measurements showed that the sealing quality was better for the anodic films formed in TSA than in DSA in agreement with the lower pore volume of the anodic films formed in TSA.
3. The corrosion behavior evaluated by EIS measurements revealed that the sealed films formed in TSA are significantly more resistant to corrosion than the sealed films formed in DSA. This enhancement of corrosion resistance is mainly associated with the higher compactness of the porous layer and higher resistance of the barrier layer obtained after hydrothermal sealing of specimens anodized in TSA.

This work showed the beneficial effect of tartaric acid addition in sulfuric acid baths for the improvement of the corrosion resistance of the anodic films, which was clearly seen after hydrothermal sealing. In addition, this study pointed out the complementarity of FESEM observations and EIS measurements to obtain a better knowledge of anodic film behavior.

Acknowledgments

This work was carried out with the technical and financial support of the Délégation Générale pour l'Armement and the European Aeronautic Defence and Space Company. In addition, we thank D. Oquab and Y. Thebault for time on the JEOL JSM 6700F FESEM instruments.

Centre National de la Recherche Scientifique assisted in meeting the publication costs of this article.

References

1. E. Eichinger, J. Osborne, and T. Van Cleave, *Met. Finish.*, **95**, 36 (1997).
2. V. Moutarlier, M. P. Gigandet, L. Ricq, and J. Pagetti, *Appl. Surf. Sci.*, **183**, 1 (2001).
3. V. Moutarlier, M. P. Gigandet, J. Pagetti, and B. Normand, *Surf. Coat. Technol.*, **161**, 267 (2002).
4. G. E. Thompson, L. Zhang, C. J. E. Smith, and P. Skeldon, *Corrosion (Houston)*, **55**, 1052 (1999).
5. L. Domingues, J. C. S. Fernandes, M. Da Cunha Belo, M. G. S. Ferreira, and L. Guerra-Rosa, *Corros. Sci.*, **45**, 149 (2003).
6. G. W. Critchlow, K. A. Yendall, D. Bahrani, A. Quinn, and F. Andrews, *Int. J. Adhes. Adhes.*, **26**, 419 (2006).
7. K. J. Kallenborn and J. R. Emmons, *NASA Conf. Publ.*, **3298**, 267 (1995).
8. A. Dattilo, S. Tamiro, and C. Romero, European Pat. EP1 233 084 A2 (2002).
9. S. Ono, M. Saito, and H. Asoh, *Electrochim. Acta*, **51**, 827 (2005).
10. G. Gorokh, A. Mozalev, D. Solovei, V. Khatko, E. Llobet, and X. Correig, *Electrochim. Acta*, **52**, 1771 (2006).
11. L. Iglesias-Rubianes, S. J. Garcia-Vergara, P. Skeldon, G. E. Thompson, J. Ferguson, and M. Beneke, *Electrochim. Acta*, **52**, 7148 (2007).
12. V. Marzocchi, L. Iglesias-Rubianes, G. E. Thompson, and F. Bellucci, *Corrosion Reviews*, **25**, 461 (2007).
13. J. A. Gonzalez, V. Lopez, E. Otero, and A. Bautista, *J. Electrochem. Soc.*, **147**, 984 (2000).
14. V. Lopez, M. J. Bartolomé, E. Escudero, E. Otero, and J. A. González, *J. Electrochem. Soc.*, **153**, B75 (2006).
15. M. J. Bartolomé, V. Lopez, E. Escudero, and J. A. González, *Revista de Metalurgia*, **43**, 209 (2007).
16. T. P. Hoar and G. C. Wood, *Electrochim. Acta*, **7**, 333 (1962).
17. J. Hitzig, K. Jüttner, W. J. Lorenz, and W. Paatsch, *J. Electrochem. Soc.*, **133**, 887 (1986).
18. F. Mansfeld and M. W. Kendig, *J. Electrochem. Soc.*, **135**, 828 (1988).
19. N. Celati, M. C. Sainte Catherine, M. Keddani, and H. Takenouti, *Mater. Sci. Forum*, **192**, 335 (1995).
20. J. A. González, V. Lopez, A. Bautista, and E. Otero, *J. Appl. Electrochem.*, **29**, 229 (1999).

21. J. J. Suay, E. Giménez, T. Rodríguez, K. Habib, and J. J. Saura, *Corros. Sci.*, **45**, 611 (2003).
22. M. Curioni, M. Saenz de Miera, P. Skeldon, G. E. Thompson, and J. Ferguson, *J. Electrochem. Soc.*, **155**, C387 (2008).
23. G. E. Thompson, *Thin Solid Films*, **297**, 192 (1997).
24. Y. Liu, P. Skeldon, G. E. Thompson, H. Habazaki, and K. Shimizu, *Corros. Sci.*, **44**, 1133 (2002).
25. T. Dimogerontakis, L. Kompotiatis, and I. Kaplanoglou, *Corros. Sci.*, **40**, 1939 (1998).
26. X. Zhou, G. E. Thompson, H. Habazaki, M. A. Paez, K. Shimizu, P. Skeldon, and G. C. Wood, *J. Electrochem. Soc.*, **147**, 1747 (2000).
27. M. A. Paez, O. Bustos, G. E. Thompson, P. Skeldon, K. Shimizu, and G. C. Wood, *J. Electrochem. Soc.*, **147**, 1015 (2000).
28. S. J. Garcia-Vergara, K. El Khazmi, P. Skeldon, and G. E. Thompson, *Corros. Sci.*, **48**, 2937 (2006).
29. G. A. Dorsey, *J. Electrochem. Soc.*, **113**, 169 (1966).
30. G. A. Dorsey, *J. Electrochem. Soc.*, **113**, 172 (1966).
31. G. A. Dorsey, *J. Electrochem. Soc.*, **113**, 284 (1966).
32. G. J. Brug, A. L. G. Van Den Eeden, M. Sluyters-Rehbach, and J. H. Sluyters, *J. Electroanal. Chem. Interfacial Electrochem.*, **176**, 275 (1984).
33. R. C. Spooner and W. J. Forsyth, *Plating*, **55**, 336 (1968).
34. R. C. Spooner and W. J. Forsyth, *Plating*, **55**, 341 (1968).
35. R. C. Spooner and W. J. Forsyth, *Plating*, **55**, 463 (1968).
36. K. Wefers, *Aluminium*, **49**, 553 (1973).
37. K. Wefers, *Aluminium*, **49**, 622 (1973).
38. L. Hao and B. R. Cheng, *Met. Finish.*, **98**, 8 (2000).
39. M. J. Bartolomé, V. Lopez, E. Escudero, G. Caruana, and J. A. Gonzalez, *Surf. Coat. Technol.*, **200**, 4530 (2006).
40. A. Lasia, *J. Electroanal. Chem.*, **428**, 155 (1997).
41. K. Shimizu, H. Habazaki, P. Skeldon, G. E. Thompson, and G. C. Wood, *Electrochim. Acta*, **45**, 1805 (2000).